ACS OMEGA

Open Access

http://pubs.acs.org/journal/acsodf

Article

Evaluation of the Binding Mechanism of Dietary Phytochemical, Ellagic Acid, with Human Transferrin: Spectroscopic, Calorimetric, and Computational Approaches Targeting Neurodegenerative Diseases

Mohammed Alrouji, Fahad A. Alhumaydhi, Mohammad Furkan, Kumar Venkatesan, Sharaf E. Sharaf, Moyad Shahwan, Rizwan Hasan Khan,* and Anas Shamsi*

Cite This: *ACS Omega* 2024, 9, 16089−16096

Read Online

ACCESS | Metrics & More | Article Recommendations

ABSTRACT: Human transferrin (Htf) is vital in maintaining iron within the brain cells; any disruption results in the development of neurodegenerative diseases (NDs) and other related pathologies, especially Alzheimer's disease (AD). Ellagic acid (EA), a naturally occurring phenolic antioxidant, possesses neuroprotective potential and is present in a broad variety of fruits and vegetables. The current work explores the binding mechanism of dietary polyphenol, EA, with Htf by a combination of experimental and computational approaches. Molecular docking studies unveiled the binding of EA to Htf with good affinity. Molecular dynamic (MD) simulation further provided atomistic details of the binding process, demonstrating a stable Htf−EA complex formation without causing substantial alterations to the protein's conformation. Furthermore, fluorescence binding measurements indicated that EA forms a high-affinity interaction with Htf. Isothermal titration calorimetric measurements advocated the spontaneous nature of binding and also revealed the binding process to be exothermic. In conclusion, the study deciphered the binding mechanism of EA with Htf. The results demonstrated that EA binds with Htf with an excellent affinity spontaneously, thereby laying the groundwork for potential applications of EA in the realm of therapeutics for NDs in the context of iron homeostasis.

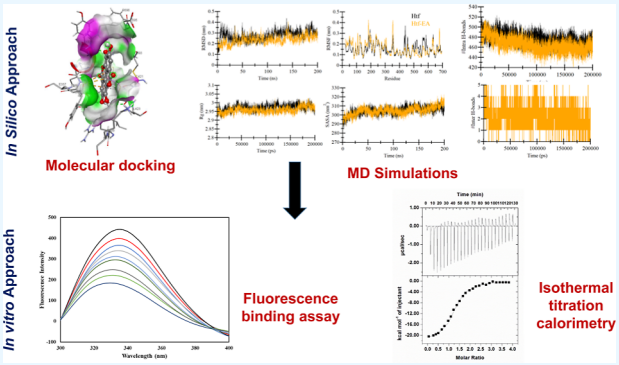

1. INTRODUCTION

Neurodegenerative diseases (NDs) are a major concern for public well-being in contemporary times. The main contributory factor of NDs like Parkinson's disease (PD) and Alzheimer's disease (AD) results from scarcity of effective therapies; nevertheless, an increasing number of supportive and therapeutic choices are becoming available.[1] AD involves degeneration of the brains' healthy neurons and is among the most prevalent dementia that affects million individuals across the globe.[2] A pathogenic hallmark protein of AD is amyloid β, which accumulates, resulting in extracellular plaques formation. Numerous cellular processes are impacted by these plaques, from changes in the regulatory checks of "calcium signaling systems" to the production of "reactive oxygen species" (ROS) and "reactive nitrogen species" (RNS).[3] The formation of neurofibrillary tangles is the second main pathological characteristic of AD that results from hyperphosphorylation of the tau protein, leading to microtubule instability. According to current research, growing evidence suggests that neuroinflammation plays a significant pathogenic role in AD. Strong evidence of a link between AD pathogenesis and neuroinflammation has been reported in several recent studies; a recent research found that the brain's inflammatory response played a primary role in AD pathogenesis.[4]

Pro-inflammatory mediators were found in large amounts in the brains of AD patients. The cells that form the central nervous system are called astrocytes and microglia, and they are essential to both function and illness. In the early phases of neurodegeneration, glial activation functions as a protective mechanism to regulate tissue repair. However, prolonged and needless activation results in a chronic neuroinflammatory response, which is linked to the initiation and progression of a majority of NDs, including AD, PD, and amyotrophic lateral

Received: December 7, 2023
Revised: March 4, 2024
Accepted: March 13, 2024
Published: March 29, 2024

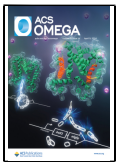

sclerosis. Inflammatory mediators such as chemokines, cytokines, "ROS", "RNS", and others are created as a result of microglia and astrocyte activation. This milieu of neuroinflammation eventually leads to neuronal death.[5]

Ellagic acid (EA) is a naturally occurring phenolic antioxidant that is present in a broad variety of fruits and vegetables. According to recent research, EA has the potential to inhibit or delay the progression of NDs by activating various cellular pathways. EA has strong neuroprotective benefits that can be attributed to its ability to scavenge free radicals, potential to chelate iron, and lessen mitochondrial malfunction. Additionally, EA is a neuroprotective agent that can lessen brain damage and improve memory and neuronal function. Cytology and histopathology experiments have demonstrated the therapeutic potential of EA for a number of neurological conditions including AD, PD, and cerebral ischemia.

Free iron is a potent neurotoxic that may cause oxidative stress by generating ROS.[6] Since oxidative stress is a major pathogenic component of neurodegeneration, iron in its free form is a powerful neurotoxic. One of the main pathogenic characteristics of NDs is oxidative stress, which is produced by extremely reactive radicals, namely, hydroxyl radicals, which are produced by the Fenton reaction and have the ability to harm DNA, proteins, and lipids and eventually cause cell death. Through their interactions with iron-regulatory proteins, the production of "ROS" and "RNS", which are directly related to the inflammatory process, can have a substantial impact on iron metabolism.

The exact cause of neuroinflammation in NDs is unknown, but a long-lasting reaction results from the activation of astrocytes and microglia. It is also evident that iron dyshomeostasis is critical for maintaining the neuroinflammatory phenotype. Along with ferritin, human transferrin (Htf) is a crucial component in maintaining proper iron levels. Htf, a vital serum plasma protein, is an essential iron transporter that binds to the endosomal compartment of cells, the transferrin receptor, and an iron complex.[7]

Pro-inflammatory cytokines will alter the iron proteins that are in charge of preserving iron homeostasis, which will increase the quantity of iron deposited in brain cells. Thus, an early neuro-inflammatory event causes iron loading in certain brain areas in AD. Therefore, the activity of iron proteins essential to maintain proper iron levels can be altered by the production of various cytokines, "ROS", and "RNS" from activated glial cells. Each of these results highlights the critical role that Htf plays in AD therapies by highlighting the significance of iron homeostasis in AD-associated neuro inflammation. Thus, the present study will be using a combination of *in vitro* and *in silico* methods to understand the binding mechanism of EA with Htf.

2. MATERIAL AND METHOD

2.1. Materials. Htf and EA were obtained from Sigma-Aldrich (St. Loius, USA). Initially, EA and Htf were dialyzed in sodium phosphate buffer, pH 7.4, to get rid of impurities (if any). For preparation of buffers, the chemicals used were of the highest grade and Milli Q water was used. Htf stock solution (5 mg/mL) was made up in 20 mM sodium phosphate buffer, pH 7.4, and further diluted to working concentrations to be used in the experiments. For spectroscopic studies, the inner filter effect was taken into consideration, and all the reported spectra are subtracted spectra.

2.2. Molecular Docking. Molecular docking was performed to understand the molecular interactions between Htf and EA. We utilized various bioinformatics software on a DELL workstation running Windows 11 for this analysis. The three-dimensional Htf structure was extracted from the Protein Data Bank (PDB ID: 3V83), and the ligand was retrieved from the PubChem database (CID: 5281855). To begin with, the extracted protein structure was refined and energy-minimized in a Swiss-PDB-Viewer.[8] The ligand was prepared using MGL tools for docking studies.[9] To facilitate the docking simulations and explore ligand−receptor interactions, we employed InstaDock software.[10] All other parameters were followed in accordance with earlier studies.[6] Following the docking simulations, the visualization was done using a Discovery Studio Visualizer[11] to have an in-depth analysis.

2.3. MD Simulations. The best pose obtained from docking studies was subjected to extensive MD simulation (200 ns) using GROMACS 2020 beta platform and charmm36-jul2022 force field.[12] The ligand parameters were produced employing the CHARMM general force field program along with the cgenff_charmm2gmx_py3_nx2.py script. The ligand was subsequently merged with Htf's original coordinates. The final systems were then placed inside a 10 Å cubic box and solvated with the SPC216 water model by means of the gmx solvate module.[13] We next carried out a phase of energy minimization using the 1500-step steepest descent algorithm. Next, the *NVT* and *NPT* ensembles were employed for running simulations for 1 ns each in order to get ready for the final MD run.

The trajectories obtained from the MD simulations were assessed with the GROMACS toolset, and XMGrace software was used to produce graphical representations.[14]

2.4. MM-PBSA Calculation. The molecular mechanics Poisson−Boltzmann surface area (MM-PBSA) methodology was used to calculate the protein−ligand complex's binding free energy.[15] The MD simulation trajectories provided the required input data for the MM-PBSA energy calculations. Specifically, a 10 ns time frame extracted from a stable segment, i.e., 50−60 ns interval of the MD trajectory, was employed for the MM-PBSA estimation. The protein−ligand complex binding free energy calculations were performed using the GROMACS suite and the gmx mmpbsa module.[16] This approach enabled a comprehensive analysis of the energetics involved in the interaction, contributing to a nuanced understanding of molecular binding events.

2.5. Fluorescence Spectroscopy. We employed a fluorescence binding study to check the actual binding of EA with Htf in line with earlier studies. EA was altered within the range of 0−5 μM, while Htf was maintained at a constant concentration of 4 μM. In accordance with prior studies, the data were entered into the modified Stern−Volmer (MSV) equation to calculate the binding constant (K) of the Htf−EA complex. We carried out the experiment in triplicate, and the mean value was taken into account. Every spectrum presented here is the subtracted spectrum, which is obtained by subtracting the blank ligand spectrum and taking into account the fluorescence of EA.

2.6. Isothermal Titration Calorimetry (ITC). A MicroCal VP-ITC 200 (Northampton, MA, USA) was utilized for conducting ITC studies, following established methodologies. To begin with, dialyzed protein (Htf) was degassed for 30 min to remove the bubbles (if any) as these bubbles lead to noise during the experimental run. After degassing, the sample cell of

https://doi.org/10.1021/acsomega.3c09792
ACS Omega 2024, 9, 16089−16096

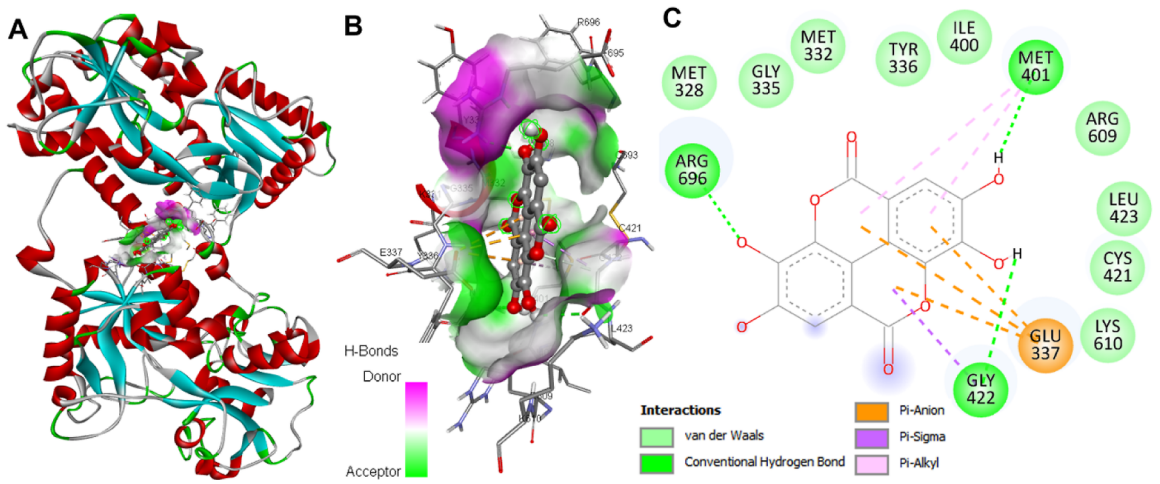

Figure 1. Analysis of interactions. (A) EA binding to Htf. (B) Cartoon depiction of EA docked with Htf. (C) Visualization of the surface potential of the Htf binding pocket occupied by EA.

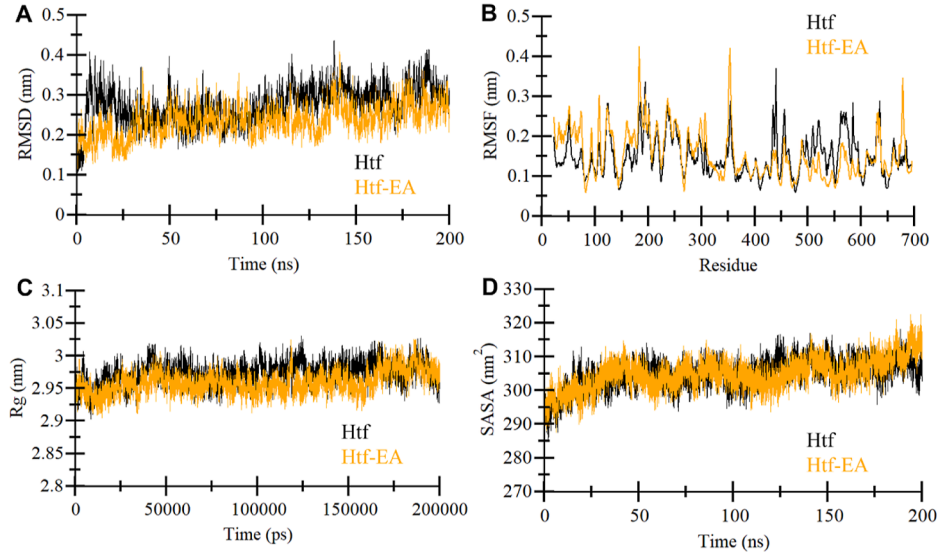

Figure 2. Exploring the structural dynamics and compactness of Htf with EA through: (A) RMSD, (B) RMSF, (C) *Rg*, and (D) SASA plots. In these plots, black corresponds to values obtained for free Htf, while orange signifies values for the Htf–EA complexes.

the instrument was filled with this degassed protein (20 μM), while the reference cell beside the sample cell was filled with the corresponding buffer. The ligand (EA) was loaded into the syringe, and a programmed titration was initiated, commencing with an initial false injection of 5 μL that is not considered in the analysis, succeeded by successive injections of EA into the sample cell containing the protein of interest (Htf), each consisting of 10 μL. The spacing was fixed at 280 s, the time length was set at 20 s, and the stirring speed was maintained at 307 rpm as the experimental settings. The final figure was obtained through the software associated with ITC apparatus MicroCal Origin 8.0 to obtain the thermodynamic parameters of the complex.

3. RESULT

3.1. Molecular Docking. Significant interactions between EA and Htf were identified by molecular docking studies. Our comprehensive examination of docking results identified the specific residues involved in the interactions, thereby demonstrating the manner in which EA interacts with Htf. A total of nine possible poses were generated in the molecular docking. The calculated binding affinity for the preferential pose was found to be −7.9 kcal/mol. EA had a notable ligand efficiency value of 0.3591 kcal/mol/non-H atom in relation to Htf. Our findings suggested that EA had a tendency to occupy Htf's iron binding pocket. As apparent in Figure 1, EA formed significant interactions with the binding pocket residues within this deep cavity. Particularly noteworthy was the presence of three hydrogen bonds between EA and Met401, Gly422, and Arg696 (Figure 1A). Surface visualizations revealed how EA occupied the iron-binding pocket within Htf's internal cavity (Figure 1B). Furthermore, we identified several key interactions, including alkyl, π–alkyl, and van der Waals forces, with several residues of Htf, stabilizing the complex (Figure 1C). According to our observations, EA binds to Htf inside the binding pocket, modulating Htf's catalytic activity.

3.2. Htf Dynamics upon EA Binding. We examined the intricate internal dynamics, physical transitions, and conformational changes in Htf after EA binding by employing all-atom MD simulations. This methodology enabled us to explore the

https://doi.org/10.1021/acsomega.3c09792
ACS Omega 2024, 9, 16089−16096

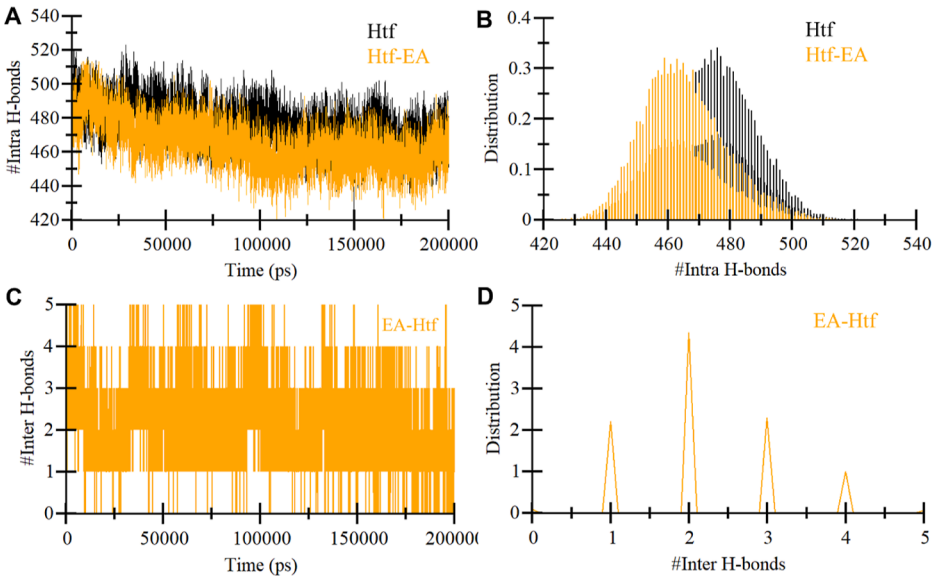

Figure 3. Temporal evolution of hydrogen bond formation: (A,B) within Htf (intra-Htf) and (C,D) between EA and Htf (EA-Htf).

interactions between these macromolecules and other molecules over a specific time frame. We performed extensive all-atom MD simulations in this study for the Htf−EA complex and free Htf protein, with each simulation lasting 200 ns. It is well-established that significant conformational changes in the three-dimensional structure of proteins are frequently induced when some foreign molecule binds to its binding pocket.[17] Root mean square deviation (RMSD) is a widely accepted metric that underscores the structural stability of a protein.[18] The results evident in the obtained RMSD plots (Figure 2A) clearly show that binding of EA does not lead to any significant alterations in native Htf structure, thereby enhancing its stability. However, in the initial stages, i.e., during the first 50 ns, few fluctuations were apparent due to the initial positioning of EA within Htf's binding pocket. Post this, no significant fluctuations were seen, and RMS equilibrium was obtained throughout the course of simulation, implicative of the stability of the Htf−EA complex.

The root mean square fluctuation (RMSF) profile (Figure 2B) suggested that there were some enhanced fluctuations in Htf's N-terminal, specifically the loop regions. Following EA binding, the RMSF plot displayed a similar pattern, thereby suggesting the stability of the complex, with only minor intermittent fluctuations observed across the N-terminal and C-terminal domains. Notably, a decrease in residual fluctuations was apparent after EA binding, specifically observed in the EA binding region. One possible explanation for this observation is the existence of more residual vibrations during the simulation in the presence of EA.

Further, we computed the radius of gyration (R_g) for free Htf and the Htf−EA complex to have an insight into the effect of EA binding on Htf's conformation; a higher value of R_g indicates less compactness. R_g plots (Figure 2C) clearly depict that average R_g values for free Htf and the Htf−EA complex stayed consistently in the range of 2.9−3.0 nm. During the course of simulation, the values were stable for Htf and pre- and post-EA binding. Overall, it is apparent from R_g plots that the binding of EA to Htf induces only minor changes and causes no major structural rearrangement, implying the stability of the Htf−EA complex. These observations are in accordance with earlier discussed RMSD and RMSF plots, reinforcing the stability of the Htf−EA complex.

Moreover, solvent-accessible surface area (SASA) was computed for free protein and the protein−ligand complex, and the obtained SASA plots were in line with earlier discussed parameters. We computed and plotted average SASA values over time for Htf and the Htf−EA complex (Figure 2D), and these were found to be in the range of 290−315 nm^2. It was apparent from the obtained plots that higher stability in SASA values was observed for the complex.

This slight decrement in SASA signifies conformational stability in Htf attributed to the binding of EA, arising from the presence of the ligand in Htf's internal cavity. This event emphasizes the way of interaction of EA with Htf; i.e., EA interacts with Htf dynamically, affecting the protein's total surface interaction with its surroundings. Altogether, the analysis of all these parameters validates the stability of the Htf−EA complex during the course of simulation.

3.3. Hydrogen Bonding Dynamics. Intramolecular hydrogen bonding is the cornerstone for maintaining the integrity of the protein structure, and thus an investigation into the dynamics of hydrogen bonds provides a unique perspective,[19] shedding light on the stability of polar interactions in these complexes.[20] We conducted an extensive analysis of the intramolecular hydrogen bonds to assess the stability of protein alone and in complex with ligand throughout the simulation (Figure 3A,B). This analysis illustrates the changes in the hydrogen bond formation in Htf in the absence and presence of EA. It was apparent that the intramolecular hydrogen bonds were steady and consistent throughout the simulation, except for a minor decrement, thereby implying that the structural integrity of Htf remains intact even post-EA binding.

Additionally, a number of conventional hydrogen bonds during the course of simulation were computed for the complex, and we found that up to 5 hydrogen bonds were formed as illustrated in Figure 3C. A constant fluctuation was on display for these hydrogen bonds of variable magnitude (4−5 hydrogen bonds); however, 1 to 3 hydrogen bonds remained relatively stable during the simulation with minimal fluctuation (Figure 3D). These results are consistent with our earlier

https://doi.org/10.1021/acsomega.3c09792
ACS Omega 2024, 9, 16089−16096

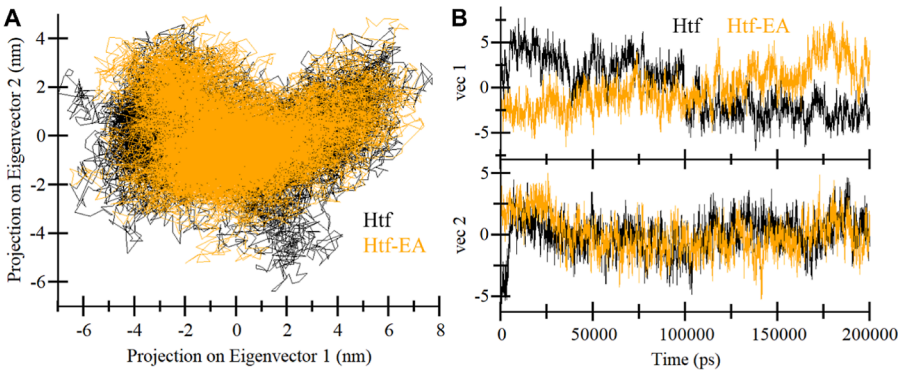

Figure 4. Principal component analysis: (A) 2D Projections of Htf conformations. (B) Time-evolution of conformations for free Htf and the Htf–EA complex.

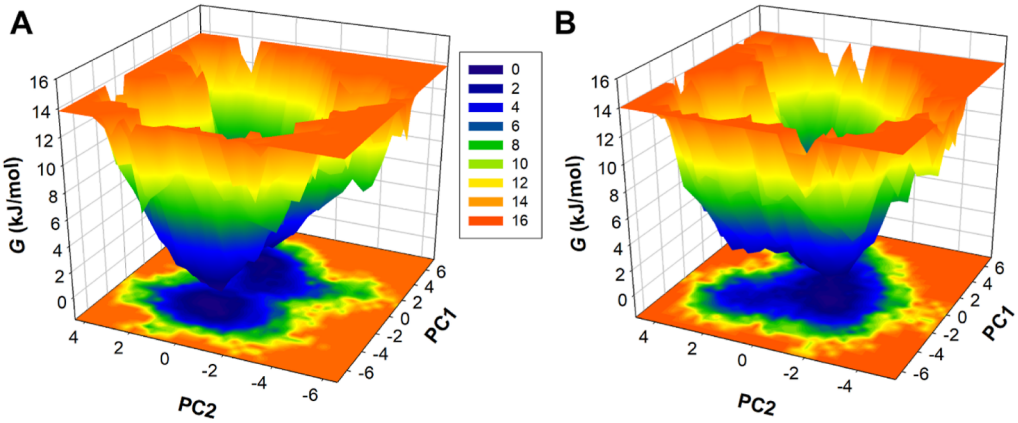

Figure 5. FEL for (A) Htf and the (B) Htf–EA complex.

molecular docking results. Collectively, these observations confirm the dynamic nature of hydrogen bond formation and fluctuation in the complex. These interactions signify their involvement in the binding pocket of Htf.

3.4. Principal Component Analysis. A widely popular method that examines the collective atomic motions of proteins is principal component analysis (PCA).[21] By identifying the primary motions depicted by "eigenvectors", PCA yields a comprehensive analysis of protein's overall dynamics, thereby giving a way to analyze its stability. In this study, we used PCA to evaluate the conformational variation of the Htf–EA complex and unbound Htf inside the critical subspace, as illustrated in Figure 4. The conformational landscape demonstrated using the projection of the Cα atom along the first and second "eigenvectors" gives a clear picture of what conformational states are adopted by the protein. A network of stable states is visible for Htf, indicating that Htf explores a similar range of phase spaces before and after EA binding. Once EA binds to Htf, no major transition occurs in Htf's motion (Figure 4B), emphasizing that this binding does not cause any major transition in the native Htf conformation.

3.5. Free Energy Landscape Analysis. Further, we moved toward the free energy landscape (FEL) for protein alone and in combination with the ligand to shed more light on the effect of EA binding on the Htf's folding and dynamics. Figure 5 illustrates the FELs of free Htf and the Htf–EA complex. The FEL of free protein shows two adjutant stable global minima, primarily concentrated in 1–2 basins (Figure 5A). On the contrary, when EA binds to Htf, a noticeable shift in conformation occurred, evident from the broader energy minimum of the complex (Figure 5B). The FEL of the complex shows a single stable global minimum, mainly centered within a single basin (Figure 5B). FEL analysis clearly suggests that a modification is induced in the energy landscape of Htf upon EA binding, thereby giving rise to a distinct conformational state. These findings significantly enrich our understanding of the conformational landscape and possible functional consequences of free Htf and the Htf–EA complex in the presence of EA.

3.6. MM-PBSA Analysis. In order to gain a deeper understanding of the forces governing Htf–EA interaction, we used the MM-PBSA approach to compute free energies.[22] From a stable region within the 10 ns molecular dynamics trajectories, we selected a frame for the MM-PBSA estimation. The results revealed a favorable binding of EA to Htf, showcasing a negative binding free energy of −92.18 kJ/mol. The negativity was predominantly caused by electrostatic contacts, nonpolar solvation energy, and van der Waals forces, whereas polar solvation energy contributed positively to the overall binding energy. These findings highlight EA as a promising candidate against Htf. The consistent agreement with various simulation analyses enhances the robustness of our conclusions and validates the stability of the Htf–EA complex.

3.7. Fluorescence Spectroscopy. Fluorescence spectroscopy is a vital technique that validates the actual binding of a ligand with the protein. The origin of fluorescence in proteins can be attributed to three intrinsic fluorophores within the molecular structure: tryptophan emerging as the predominant contributor to this phenomenon. For Htf, tryptophan alone is

https://doi.org/10.1021/acsomega.3c09792
ACS Omega 2024, 9, 16089−16096

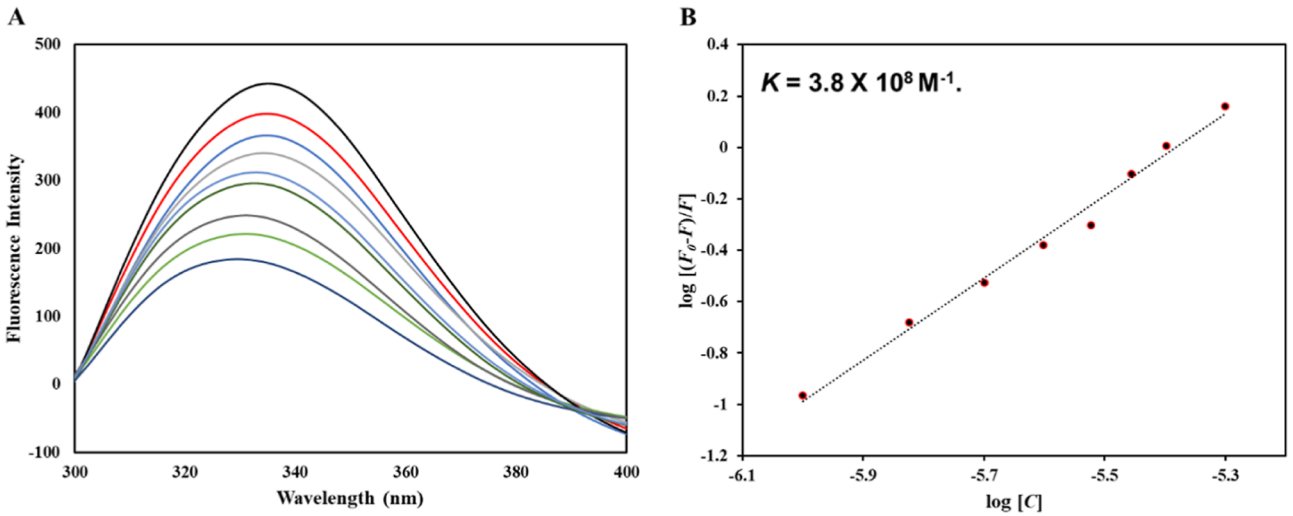

Figure 6. Fluorescence binding studies. (A) Fluorescence spectra of native Htf and in the presence of EA (0−5 μM). (B) MSV plot of the Htf−EA complex.

the main contributor to the intrinsic fluorescence. Tyrosine's fluorescence is completely quenched when subjected to ionization or when in proximity to an amino group, a carboxyl group, or another tryptophan residue. On the contrary, phenylalanine has a very low quantum yield. To further validate the computational observations with experimental approaches, we deployed fluorescence spectroscopy (Figure 6). The intrinsic fluorescence of Htf exhibits high sensitivity to its microenvironment.[23] and thus subtle alterations in the microenvironment around its fluorophores correlates with alterations in the fluorescence spectra. When Htf was excited at 280 nm, it displayed an emission maximum at around 335 nm, implying that Htf is in its native form (Figure 6A). Fluorescence quenching is the name given to the phenomena when a commensurate drop in fluorescence intensity occurs with increasing concentrations of ligand; Htf's fluorescence intensity decreased with increasing EA concentrations (Figure 6A). This dose-dependent decrease in the fluorescence intensity in the presence of EA is suggestive of the formation of the Htf−EA complex, validating our *in silico* observations. The binding constant (K) of the complex was obtained by fitting the quenching data into the MSV equation to generate the MSV plot (Figure 6B). EA demonstrated excellent binding with Htf with a binding constant of 3.8×10^8 M^{-1}. The computed K value is much higher than that reported for other protein−ligand complexes, indicating excellent strength of the interaction between EA and Htf. In conclusion, fluorescence spectroscopy along with molecular docking and molecular dynamics simulation approaches affirms the formation of a stable Htf−EA complex.

3.8. Isothermal Titration Calorimetry. ITC is one of the most sensitive techniques for studying protein−ligand binding and determining the thermodynamic characteristics of the complex. After finding out through fluorescence spectroscopy that EA displays an exceptional affinity for binding to Htf, we conducted ITC to unveil binding energetics associated with the Htf−EA complex and also to shed light on the molecular forces that are driving the complex formation. An individual injection of the compound (EA) into the target protein (Htf) corresponds to each peak in the ITC isotherm (upper panel) of Figure 7, which also displays the integrated plot of heat released per injection as a function of the molar ratio of ligand

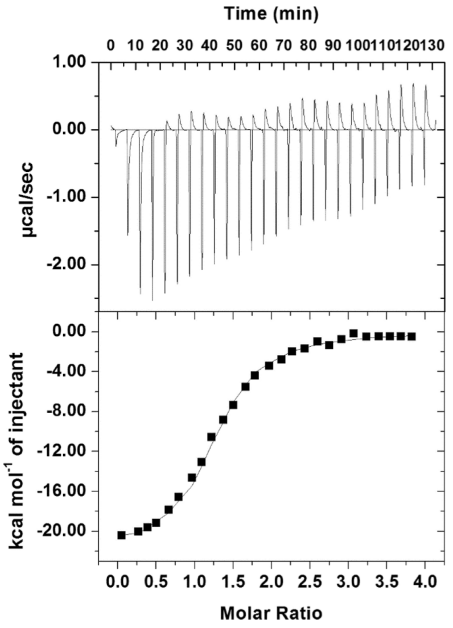

Figure 7. ITC isotherm of the Htf−EA complex. The upper panel illustrates the raw data from the sequential titration of EA into the sample cell containing 20 μM Htf. The lower panel shows the calorimetric titration's integrated heat results after accounting for heat of dilution against molar ratio.

to protein in the lower panel (Figure 7). It is apparent from the obtained isotherm that EA binds to Htf spontaneously, and moreover, a negative heat of deflection is observed, which implies that the binding of EA with Htf is exothermic. All the parameters obtained for the Htf−EA complex are shown in Table 1. Thus, ITC observations correlate with spectroscopic observations and validate the in silico observations, affirming the excellent binding of EA with Htf resulting in the formation of a stable Htf−EA complex.

4. DISCUSSION

In this study, computational and experimental approaches were used to have a detailed insight into binding of EA with Htf. Molecular docking and molecular dynamics (MD) simulation

https://doi.org/10.1021/acsomega.3c09792
ACS Omega 2024, 9, 16089−16096

Table 1. Thermodynamic Parameters obtained from ITC for the Htf–EA Complex

Htf–EA complex		
K_a (association constant) M^{-1}	ΔH (enthalpy change)cal/mol	ΔS (cal/mol/deg)
$K_a = 6.90 \times 105 \pm 7.5 \times 101$	$\Delta H = -2.20 \times 104 \pm 434$	$\Delta S = -47.2$

techniques allowed us to explore the binding mode, stability, and dynamic behavior of the Htf–EA complex. Strong evidence of an interaction between EA and Htf was established by using molecular docking studies, indicating that Htf has the potential to be a meaningful binding partner. Specifically, EA occupied the iron-binding pocket of Htf and established vital hydrogen bonds with important residues, such as Met401, Gly422, and Arg696, shedding light on the binding mechanism. Further, MD simulations provided atomistic insights into the structural dynamics of the complex over an extended 200 ns period. The results from MD analysis revealed that EA binds to Htf efficiently, forming a stable complex; i.e., binding of EA induces minimal structural alterations in the Htf structure, forming a stable complex. Further, fluorescence binding assay demonstrated that EA binds to Htf with excellent affinity; a binding constant of the order of 10^8 M^{-1} suggests the intensity of the interaction. Further, ITC analysis deciphered the spontaneous binding of EA with Htf. Overall, the study extensively explored the binding and dynamic behavior of the Htf–EA complex, utilizing integrated experimental and computational approaches. The identified binding mechanism and observed structural stability form a robust foundation for future studies aiming to harness EA's therapeutic potential in addressing NDs in the context of iron homeostasis.

■ ASSOCIATED CONTENT

Data Availability Statement

The information supporting this study is available in this article.

■ AUTHOR INFORMATION

Corresponding Authors

Rizwan Hasan Khan − *Interdisciplinary Biotechnology Unit, Aligarh Muslim University, Aligarh 202002, India*; Email: rizwanhkhan1@gmail.com

Anas Shamsi − *Centre of Medical and Bio-allied Health Sciences Research, Ajman University, Ajman 346, United Arab Emirates*; orcid.org/0000-0001-7055-7056; Email: anas.shamsi18@gmail.com

Authors

Mohammed Alrouji − *Department of Medical Laboratories, College of Applied Medical Sciences, Shaqra University, Shaqra 11961, Saudi Arabia*

Fahad A. Alhumaydhi − *Department of Medical Laboratories, College of Applied Medical Sciences, Qassim University, Buraydah 52571, Saudi Arabia*; orcid.org/0000-0002-0151-8309

Mohammad Furkan − *Department of Biochemistry, Aligarh Muslim University, Aligarh 202002, India*

Kumar Venkatesan − *Department of Pharmaceutical Chemistry, College of Pharmacy, King Khalid University, Abha 62529, Saudi Arabia*

Sharaf E. Sharaf − *Pharmaceutical Sciences Department, College of Pharmacy, Umm Al-Qura University, Makkah 21421, Saudi Arabia*

Moyad Shahwan − *Centre of Medical and Bio-allied Health Sciences Research, Ajman University, Ajman 346, United Arab Emirates*

Complete contact information is available at: https://pubs.acs.org/10.1021/acsomega.3c09792

Author Contributions

Conceptualization, A.S. and R.H.K.; data curation, M.A., M.S., K.V. and F.A.A.; formal analysis, A.S., M.F. and R.H.K.; funding acquisition, ANAS SHAMSI; investigation, M.A., K.V. and S.E.S.; methodology, A.S., M.F., M.A.; project administration, A.S. and R.H.K.; resources, A.S., M.S. and R.H.K.; software, A.S., M.A. and S.E.S.; validation, A.S.; visualization, M.F. and M.A.; writing–original draft, ANAS SHAMSI, M.F. and M.A.; writing–review and editing, R.H.K. and M.S.

Notes

The authors declare no competing financial interest.

■ ACKNOWLEDGMENTS

The authors extend their appreciation to the Deanship of Scientific Research at King Khalid University for funding this work through Large Groups Project under grant number (RGP.2/125/44). M.A. is thankful to the Deanship of Scientific Research at Shaqra University for supporting this work. The authors are also grateful to Ajman University, UAE, for providing all the necessary facilities and supporting the publication.

■ REFERENCES

(1) (a) Wilson, D. M.; Cookson, M. R.; Van Den Bosch, L.; Zetterberg, H.; Holtzman, D. M.; Dewachter, I. Hallmarks of neurodegenerative diseases. *Cell* **2023**, *186* (4), 693–714. (b) Zahra, W.; Rai, S. N.; Birla, H.; Singh, S. S.; Dilnashin, H.; Rathore, A. S.; Singh, S. P. The global economic impact of neurodegenerative diseases: Opportunities and challenges. *Bioeconomy for Sustainable Development*; Springer, 2020; pp 333–345.

(2) (a) Reitz, C.; Brayne, C.; Mayeux, R. Epidemiology of Alzheimer disease. *Nat. Rev. Neurol.* **2011**, *7* (3), 137–152. (b) Olajide, O. A.; Sarker, S. D. Alzheimer's disease: natural products as inhibitors of neuroinflammation. *Inflammopharmacology* **2020**, *28* (6), 1439–1455.

(3) (a) Poirier, J.; Bertrand, P.; Poirier, J.; Kogan, S.; Gauthier, S.; Poirier, J.; Gauthier, S.; Davignon, J.; Bouthillier, D.; Davignon, J. Apolipoprotein E polymorphism and Alzheimer's disease. *Lancet* **1993**, *342* (8873), 697–699. (b) De Strooper, B.; Iwatsubo, T.; Wolfe, M. S. Presenilins and γ-secretase: structure, function, and role in Alzheimer disease. *Cold Spring Harb. Perspect. Med.* **2012**, *2* (1), a006304. (c) Balez, R.; Steiner, N.; Engel, M.; Muñoz, S. S.; Lum, J. S.; Wu, Y.; Wang, D.; Vallotton, P.; Sachdev, P.; O'Connor, M.; et al. Neuroprotective effects of apigenin against inflammation, neuronal excitability and apoptosis in an induced pluripotent stem cell model of Alzheimer's disease. *Sci. Rep.* **2016**, *6* (1), 31450.

(4) (a) Dourado, N. S.; Souza, C. d. S.; De Almeida, M. M. A.; Bispo da Silva, A.; Dos Santos, B. L.; Silva, V. D. A.; De Assis, A. M.; da Silva, J. S.; Souza, D. O.; Costa, M. d. F. D.; et al. Neuroimmunomodulatory and neuroprotective effects of the flavonoid apigenin in in vitro models of neuroinflammation associated with Alzheimer's disease. *Front. Aging Neurosci.* **2020**, *12*, 119. (b) Wang, J.-z.; Wu, Q.; Smith, A.; Grundke-Iqbal, I.; Iqbal, K. τ is phosphorylated by GSK-3 at several sites found in Alzheimer disease and its biological activity markedly inhibited only after it is prephosphorylated by A-kinase. *FEBS Lett.* **1998**, *436* (1), 28–34. (c) Heppner, F. L.; Ransohoff, R. M.; Becher, B. Immune attack: the

https://doi.org/10.1021/acsomega.3c09792
ACS Omega 2024, 9, 16089–16096

role of inflammation in Alzheimer disease. *Nat. Rev. Neurosci.* **2015**, *16* (6), 358−372. (d) Fu, W.-Y.; Wang, X.; Ip, N. Y. Targeting neuroinflammation as a therapeutic strategy for Alzheimer's disease: mechanisms, drug candidates, and new opportunities. *ACS Chem. Neurosci.* **2019**, *10* (2), 872−879.

(5) (a) Streit, W. J. Microglia and neuroprotection: implications for Alzheimer's disease. *Brain Res. Rev.* **2005**, *48* (2), 234−239. (b) Kraft, A. D.; Harry, G. J. Features of microglia and neuroinflammation relevant to environmental exposure and neurotoxicity. *Int. J. Environ. Res. Publ. Health* **2011**, *8* (7), 2980−3018. (c) Heneka, M. T.; Carson, M. J.; Khoury, J. E.; Landreth, G. E.; Brosseron, F.; Feinstein, D. L.; Jacobs, A. H.; Wyss-Coray, T.; Vitorica, J.; Ransohoff, R. M.; et al. Neuroinflammation in Alzheimer's disease. *Lancet Neurol.* **2015**, *14* (4), 388−405. (d) Ghadery, C.; Koshimori, Y.; Coakeley, S.; Harris, M.; Rusjan, P.; Kim, J.; Houle, S.; Strafella, A. P. Microglial activation in Parkinson's disease using [18 F]-FEPPA. *J. Neuroinflammation* **2017**, *14*, 8−9. (e) Shi, Y.; Holtzman, D. M. Interplay between innate immunity and Alzheimer disease: APOE and TREM2 in the spotlight. *Nat. Rev. Immunol.* **2018**, *18* (12), 759−772. (f) McCauley, M. E.; Baloh, R. H. Inflammation in ALS/FTD pathogenesis. *Acta Neuropathol.* **2019**, *137* (5), 715−730.

(6) Xue, B.; DasGupta, D.; Alam, M.; Khan, M. S.; Wang, S.; Shamsi, A.; Islam, A.; Hassan, M. I. Investigating binding mechanism of thymoquinone to human transferrin, targeting Alzheimer's disease therapy. *J. Cell. Biochem.* **2022**, *123* (8), 1381−1393.

(7) (a) Khan, S.; Cho, W. C.; Hussain, A.; Azimi, S.; Babadaei, M. M. N.; Bloukh, S. H.; Edis, Z.; Saeed, M.; Ten Hagen, T. L.; Ahmadi, H.; et al. The interaction mechanism of plasma iron transport protein transferrin with nanoparticles. *Int. J. Biol. Macromol.* **2023**, *240*, 124441. (b) Hadzhieva, M.; Kirches, E.; Mawrin, C. Review: Iron metabolism and the role of iron in neurodegenerative disorders. *Neuropathol. Appl. Neurobiol.* **2014**, *40* (3), 240−257.

(8) Kaplan, W.; Littlejohn, T. G. Swiss-PDB viewer (deep view). *Briefings Bioinf.* **2001**, *2* (2), 195−197.

(9) Huey, R.; Morris, G. M.; Forli, S. *Using AutoDock 4 and AutoDock vina with AutoDockTools: a tutorial*; Scripps Research Institute Molecular Graphics Laboratory, 2012; Vol. *10550* (92037), p 1000.

(10) Mohammad, T.; Mathur, Y.; Hassan, M. I. InstaDock: A single-click graphical user interface for molecular docking-based virtual high-throughput screening. *Briefings Bioinf.* **2021**, *22* (4), bbaa279.

(11) Biovia, D. S. *Discovery Studio Visualizer*; BIOVIA: *San Diego, CA, USA*, 2017; Vol. *936*.

(12) (a) Van Der Spoel, D.; Lindahl, E.; Hess, B.; Groenhof, G.; Mark, A. E.; Berendsen, H. J. GROMACS: fast, flexible, and free. *J. Comput. Chem.* **2005**, *26* (16), 1701−1718. (b) Huang, J.; MacKerell, A. D., Jr. CHARMM36 all-atom additive protein force field: Validation based on comparison to NMR data. *J. Comput. Chem.* **2013**, *34* (25), 2135−2145.

(13) Glättli, A.; Daura, X.; van Gunsteren, W. F. Derivation of an improved simple point charge model for liquid water: SPC/A and SPC/L. *J. Chem. Phys.* **2002**, *116* (22), 9811−9828.

(14) Turner, P. XMGRACE, Version 5.1. 19. *Center for Coastal and Land-Margin Research*; Oregon Graduate Institute of Science and Technology: Beaverton, OR, 2005; Vol. *2*.

(15) Homeyer, N.; Gohlke, H. Free energy calculations by the molecular mechanics Poisson- Boltzmann surface area method. *Mol. Inf.* **2012**, *31* (2), 114−122.

(16) Valdés-Tresanco, M. S.; Valdés-Tresanco, M. E.; Valiente, P. A.; Moreno, E. gmx_MMPBSA: a new tool to perform end-state free energy calculations with GROMACS. *J. Chem. Theory Comput.* **2021**, *17* (10), 6281−6291.

(17) Mohammad, T.; Siddiqui, S.; Shamsi, A.; Alajmi, M. F.; Hussain, A.; Islam, A.; Ahmad, F.; Hassan, M. I. Virtual screening approach to identify high-affinity inhibitors of serum and glucocorticoid-regulated kinase 1 among bioactive natural products: Combined molecular docking and simulation studies. *Molecules* **2020**, *25* (4), 823.

(18) Pitera, J. W. Expected distributions of root-mean-square positional deviations in proteins. *J. Phys. Chem. B* **2014**, *118* (24), 6526−6530.

(19) Menéndez, C. A.; Accordino, S. R.; Gerbino, D. C.; Appignanesi, G. A. Hydrogen bond dynamic propensity studies for protein binding and drug design. *PLoS One* **2016**, *11* (10), No. e0165767.

(20) J R Yunta, M. It is important to compute intramolecular hydrogen bonding in drug design. *Am. J. Model. Optim.* **2017**, *5* (1), 24−57.

(21) Stein, S. A. M.; Loccisano, A. E.; Firestine, S. M.; Evanseck, J. D. Chapter 13 Principal Components Analysis: A Review of its Application on Molecular Dynamics Data. *Annu. Rep. Comput. Chem.* **2006**, *2*, 233−261.

(22) Wang, E.; Sun, H.; Wang, J.; Wang, Z.; Liu, H.; Zhang, J. Z.; Hou, T. End-point binding free energy calculation with MM/PBSA and MM/GBSA: strategies and applications in drug design. *Chem. Rev.* **2019**, *119* (16), 9478−9508.

(23) Sarzehi, S.; Chamani, J. Investigation on the interaction between tamoxifen and human holo-transferrin: determination of the binding mechanism by fluorescence quenching, resonance light scattering and circular dichroism methods. *Int. J. Biol. Macromol.* **2010**, *47* (4), 558−569.

https://doi.org/10.1021/acsomega.3c09792
ACS Omega 2024, 9, 16089−16096